

Bi-LORA: A Vision-Language Approach for Synthetic Image Detection

Mamadou Keita, Wassim Hamidouche, Hessen Bougueffa Eutamene, Abdenour Hadid, Abdelmalik Taleb-Ahmed

Abstract—Advancements in deep image synthesis techniques, such as generative adversarial networks (GANs) and diffusion models (DMs), have ushered in an era of generating highly realistic images. While this technological progress has captured significant interest, it has also raised concerns about the potential difficulty in distinguishing real images from their synthetic counterparts. This paper takes inspiration from the potent convergence capabilities between vision and language, coupled with the zero-shot nature of vision-language models (VLMs). We introduce an innovative method called Bi-LORA that leverages VLMs, combined with low-rank adaptation (LORA) tuning techniques, to enhance the precision of synthetic image detection for unseen model-generated images. The pivotal conceptual shift in our methodology revolves around reframing binary classification as an image captioning task, leveraging the distinctive capabilities of cutting-edge VLM, notably bootstrapping language image pre-training (BLIP)2. Rigorous and comprehensive experiments are conducted to validate the effectiveness of our proposed approach, particularly in detecting unseen diffusion-generated images from unknown diffusion-based generative models during training, showcasing robustness to noise, and demonstrating generalization capabilities to GANs. The obtained results showcase an impressive average accuracy of 93.41% in synthetic image detection on unseen generation models. The code and models associated with this research can be publicly accessed at <https://github.com/Mamadou-Keita/VLM-DETECT>

Index Terms—Deepfake, Text-to-Image Generation, Visual Language Model, Large Language Model, Image Captioning, Generative Adversarial Nets, Diffusion Models, Low Rank Adaptation.

I. INTRODUCTION

THE rapid progress in generative models has ushered in a new era of image synthesis, marked by the effortless creation of remarkably realistic images. This technological progress, while undeniably impressive, has also given rise to significant concerns regarding the widespread distribution of fake images. These artificial intelligence (AI)-synthesized images, due to their unrivalled visual fidelity, represent a substantial threat to various facets of society. Noteworthy examples, such as the generation of realistic face images through techniques like generative adversarial networks (GANs) and diffusion models (DMs), have reached a point where they challenge human perception and erode trust in a number

of areas, including social media, politics, the military, and cybersecurity.

The pressing issue of discerning between authentic and AI-generated images is underscored by the remarkable realism achieved by contemporary generative models, surpassing human perceptual capabilities. As demonstrated in a quantitative study by Lu *et al.* [1], human observers grapple with distinguishing genuine images from their AI-generated counterparts, achieving an accuracy rate as low as 61.3%. This challenge extends beyond academic research, permeating real-world applications, presenting both opportunities and emerging threats. The advent of text-to-image models allows users to convert textual descriptions into high-quality visual representations, a technological leap with potential malicious applications, including the spread of misinformation and propaganda. In light of these complex challenges, the primary goal is to prioritize the development of efficient detectors capable of reliably identifying fake images generated by these advanced models.

In the realm of image analysis, a myriad of techniques has been developed to detect AI-generated images. While DMs typically utilize convolutional neural networks (CNNs) or vision transformers (ViTs) as their foundational architecture, it's crucial to highlight the fundamental disparities in the underlying mechanisms driving image generation in DMs compared to their predecessors like variational autoencoders (VAEs) and GANs [2]. These distinctions in generative processes create a significant gap between detectors designed for earlier generative models and their ability to identify AI-generated images generated by diffusion models. To tackle this discrepancy, a seemingly direct approach is to train a binary classifier using CNNs or transformer-based models to distinguish diffusion-generated images from genuine ones. However, an empirical study conducted by Ricker *et al.* [3] has unveiled a fundamental weakness inherent in this approach. Despite its initial appeal, this simplistic classification framework demonstrates a serious lack of efficiency in generalizing to accurately discriminate new diffusion-generated images that have never been encountered before.

Recent years have witnessed the emergence of a new generation of powerful deep architectures in the field of computer vision. These models, often referred to as foundational models or large vision-language models (VLMs), have been trained on vast image-text datasets from the vast expanse of the internet [4]. They have made remarkable strides in terms of performance and have assumed a pivotal role in the contemporary computer vision research landscape. Situated at the intersection of natural language processing (NLP) and

Mamadou Keita, Hessen Bougueffa Eutamene and Abdelmalik Taleb-Ahmed are with Institut d'Electronique de Microélectronique et de Nanotechnologie (IEMN), UMR 8520, Université Polytechnique Hauts de France, Valenciennes, France

Wassim Hamidouche is with the Technology Innovation Institute, Abu Dhabi, UAE.

Abdenour Hadid is with the Sorbonne Center for Artificial Intelligence, Sorbonne University, Abu Dhabi, UAE.

computer vision (CV), these models bridge the gap between textual and visual data, ushering in a groundbreaking era of machine understanding. Prominent instances include CLIP [5], Flamingo [6], BLIP2 [7], Flava [8], Llava [9], SimVLM [10], Visual-BERT [11], InstructBLIP [12], and ViTGP2¹. Within the research community, there exists a substantial body of work dedicated to vision-language tasks that require the simultaneous processing of information from visual and linguistic sources to address intricate inquiries. For example, in visual question answering (VQA), an image and a corresponding question are provided as input, and the model generates an answer to the query [13]. Conversely, in image captioning, the model takes an image as input and produces a natural language description of that image [14].

In this paper, we introduce a pioneering approach for synthetic image detection, harnessing state-of-the-art VLM. Traditional methods use complex feature extraction with CNNs [15] for image classification. In contrast, our approach, named Bi-LORA, reframes the problem as image captioning, leveraging VLMs’ text generation to differentiate between real and synthetic (i.e., AI-generated) images. While a similar approach [16] adopts an alternative strategy, such as visual question answering, our focus is on generating descriptive captions for images. Specifically, we label authentic images as “true” and synthetic images as “fake”, capitalizing on the text generation capabilities of VLMs (e.g., BLIP2) combined with low-rank adaptation (LORA) tuning strategy for memory efficiency and faster training. Our primary focus is on detecting diffusion-generated images, a challenge distinct from previous generative methods like GANs. To the best of our knowledge, this work pioneers the concept of treating binary classification as image captioning, harnessing cutting-edge VLMs. Instead of binary classification, we emphasize the potential of using VLMs (e.g., BLIP2) to create informative captions indicating class membership. In summary, our work makes the following pivotal contributions:

- Reconceptualizing binary classification as image captioning: We redefine binary classification as an image captioning task, harnessing the capabilities of VLMs.
- Revealing the potential of VLMs in synthetic image detection: We shed light on the vast potential of VLMs in the realm of synthetic image detection, showcasing their robust generalization capabilities, even when faced with previously unseen diffusion-generated images.
- Empirical validation of enhanced detection: Through rigorous and comprehensive experiments, we substantiate the effectiveness of our proposed approach, particularly in the context of detecting diffusion-generated images, robustness to noise and generalization to images generated by GAN.

Our proposed approach, trained only on LSUN Bedroom and latent diffusion model (LDM) generated images, far exceeds baseline methods: ResNet50 [17], Xception [18], data-efficient image transformers (DeiT) [19], and ViTGP2. Our outstanding performance and robust generalization stem from



Fig. 1: Examples of real sample and synthetic images generated by various generators in our experiments. From left to right, Top row: Real [20], ADM [21], LDM. Middle row: DDPM [22], IDDPM [23], PNDM [24]. Bottom row: Stable Diffusion v1.4 [25], GLIDE [26], DALL-E 3 [27].

the well-aligned vision language representation of pretrained VLMs and with fewer trainable parameters. Experimental results showcase an impressive average accuracy **93.41%** in synthetic image detection.

The remainder of this paper is organized as follow. Section II provides a brief review of related works. Section III describes the proposed VLM-based approach for synthetic image detection task. Then, the performance of the proposed approach is assessed and analysed in Section IV. Finally, Section V concludes the paper.

II. RELATED WORK

In this section, we delve into the realm of synthetic image generation, providing an overview of state-of-the-art methods for both image generation and synthetic image detection.

A. Image Generation

Image generation stands at the intersection of computer vision and machine learning, focusing on the creation of synthetic images through the use of deep learning-based generative models. Prominent among these models are GANs and, more recently, DMs. The primary goal of these image generation models is to create visually realistic images that are nearly indistinguishable from real-world images. This field has experienced rapid growth, witnessing numerous advancements in recent years, thereby unlocking a spectrum of applications, including data augmentation, style transfer, and semantic manipulation.

A pioneering method for generating synthetic images was introduced by Goodfellow *et al.* [28]. This approach consists

¹<https://ankur3107.github.io/blogs/the-illustrated-image-captioning-using-transformers/>

of a generator network that generates images and a discriminator network trained to distinguish between real and AI-generated images. Since then, this framework named GANs has been successfully applied to various tasks such as face synthesis [29, 30, 31, 32, 33, 34], style transfer [35, 36, 37], and super-resolution [38, 39, 40, 41, 42]. In GAN-based image generation, significant progress has been made with the introduction of StyleGAN [31]. This architecture exploits style-based techniques to generate more realistic and compelling images. By incorporating style information into the generating network, StyleGAN gives greater control over the images generated and produces high-quality results. Several variants and extensions of GAN architectures have been proposed to meet specific challenges and tasks in the field of image generation, such as unpaired data in image generation [43], allowing control over specific image characteristics [44], and focusing on image generation without labeled data [29].

On the other hand, text-to-image generation involves processing a given text description, known as a prompt, to generate a corresponding image. Early endeavors in this domain [45, 46] utilized GANs for this purpose. These studies employed the fusion of a prompt’s embedding with a latent vector to produce an image that accurately reflects the given description. However, despite the attention garnered by numerous works [47, 48, 49, 50, 51, 52], it is essential to acknowledge that GANs do not consistently yield satisfactory generation outcomes [53, 25].

More recently, a groundbreaking architecture known as DMs [54, 26, 25, 55] has emerged, revolutionizing tasks akin to synthetic image generation. Distinguished by their ability to progressively remove noise from a signal, these models stand out for their capacity to generate exceptionally realistic images. In the realm of text-to-image generation, a provided text prompt undergoes encoding into a latent vector, guiding the transformation process from noisy images to clear and intricate representations. Several leading models, such as DALL-E [53], GLIDE [26], Midjourney [56], Imagen [55], and Stable Diffusion [25], have showcased exceptional results. These models provide unprecedented control over the image generation process, allowing users to craft highly credible images with an impressive level of detail (see Fig. 1).

B. Detection of Synthetic Images

With the rapid advancement of generative models, the need for efficient methods to detect synthetic images has become evident. While existing detectors have been effective with traditional models like GANs [28], recent progress in generative models, particularly diffusion-based architectures and the latest GAN models, presents major challenges for current detection techniques.

Recent investigations conducted in [57, 3] have studied the efficacy of existing detectors when applied to novel generative models. The outcomes of these studies indicate that current detectors encounter challenges in generalizing their performance to diffusion-based generative architectures and the latest GAN models. This limitation underscores the necessity for the development of new techniques capable of

adeptly detecting images generated by these advanced models. While substantial progress has been achieved in detecting manipulated images produced by traditional models such as GANs, the specific realm of detecting images generated by diffusion-based models remains relatively unexplored.

In their work [58], the authors employed the ResNet50 [59] model to discern between real images and those generated by AI. They introduced a detection approach that integrates both images and textual prompts, showcasing its efficacy in improving detection accuracy. This method exhibits promising potential for enhancing overall detection capabilities. Similarly, Coccomini *et al.* [60] conducted experiments utilizing straightforward deep learning models such as multi-layer perceptrons (MLPs) and common CNNs (ResNet50 [59] and XceptionNet [18]) to differentiate between real and AI-generated images. They also implemented a multimodal detector that leverages CLIP as a feature extractor from both images and their corresponding captions, followed by passing the combined features through an MLP.

Authors in [70] found that DM-generated images exhibit features that are more easily reconstructed by pre-trained DMs than natural images. In order to identify these features, they presented the diffusion reconstruction error (DIRE) utilizing the reconstruction error of images using denoising diffusion implicit models (DDIM) for inversion and reconstruction. DIRE mainly focuses on the initial x_0 timestep and might miss information from intermediate steps during diffusion and reverse diffusion. In contrast, stepwise error for diffusion-generated image detection (SeDID) [71] was introduced a novel detection method for diffusion-generated images. This technique leverages diffusion patterns’ unique properties, focusing on deterministic reverse and denoising computation errors to enhance detection accuracy. By employing the concept of (t, δ) -error with noise information during each diffusion step, SeDID method effectively differentiates real images from generated ones. Furthermore, in the work by Guarnera *et al.* [61], a multi-level method for synthetic image detection was introduced, incorporating meticulously designed training sets. This approach empowers the detector to acquire comprehensive features and comprehend hierarchical attributes. The study applied this hierarchical approach to three tasks: distinguishing real images from those generated by AI, discerning between GANs and DMs, and recognizing AI-specific architectures.

In their work, [62] investigated the enhancement of stylistic distinction by decoupling semantic and stylistic features in images. The study introduces a contrastive-based disentanglement method to analyze the role of semantics from textual descriptions and low-level perceptual cues in synthetic image detection. However, achieving semantic-style disentanglement in practice proves challenging due to the need for specialized training datasets. Additionally, authors in [65] proposed multiLID, a novel method for detecting diffusion-generated images. This approach utilizes local intrinsic dimensionality to estimate densities in CNN feature spaces, allowing the distinction of models based on their internal feature distribution densities. The process involves using an untrained ResNet18 [59] to extract low-dimensional features from synthetic images,

TABLE I: Architectures and features of state-of-the-art AI-synthesized images detection models

Authors	Architecture	Dataset	Task
Sha <i>et al.</i> [*] (2022) [58]	CNN, CLIP + MLP	DE-FAKE	binary classification
Coccomini <i>et al.</i> [*] (2023) [60]	CNN, CLIP + MLP	Diffusers	binary classification
Guarnera <i>et al.</i> [*] (2023) [61]	CNN	Level up the DeepFake detection	binary classification
Amoroso <i>et al.</i> [*] (2023) [62]	CNN	COCOFake	binary classification
Wu <i>et al.</i> [*] (2023) [63]	CLIP + MLP	LSUN, Danbooru, ProGAN, SD, BigGAN, GauGAN, styleGAN, DALLE, GLIDE, Guided Diffusion, Latent Diffusion, ImageNet, VISION, Artist, DreamBooth, Midjourney, NightCafe, StableAI, YiJian	binary classification
Xi <i>et al.</i> [*] (2023) [64]	CNN	AI-Gen Image	binary classification
Lorenz <i>et al.</i> [*] (2023) [65]	CNN + RF	CiFAKE, ArtiFact, DiffusionDB, LAION-5B, SAC, SD-v2.1, LSUN-Bedroom	binary classification
Ju <i>et al.</i> [*] (2023) [66]	CNN	LSUN, ProGAN, DF^3	binary classification
Sinita <i>et al.</i> [*] (2023) [67]	rule-based method	Laion-5B, SD v-1.4, SD v-2.1, DALL-E-Mini, GLIDE [20], DALL-E-2, MidJourney, CycleGAN, ProGAN _e , ProGAN _t , BigGAN, StyleGAN, StyleGAN2, GauGAN, StarGAN	binary classification
Guo <i>et al.</i> [*] (2023) [68]	CNN	HiFi-IFDL	binary classification
Cozzolino <i>et al.</i> [*] (2023) [69]	CLIP + SVM	ProGAN, StyleGAN2, StyleGAN3, StyleGAN-T, GigaGAN, (Score-SDE, ADM, GLIDE, eDiff-I, Latent and Stable Diffusion, DiT, DeepFloyd-IF, Stable Diffusion XL, DALL-E 2, DALL-E 3, Midjourney v5, Adobe Firefly, LSUN, FFHQ, ImageNet, COCO, LAION, RAISE	binary classification
Wang <i>et al.</i> [*] (2023) [70]	CNN	DiffusionForensics	binary classification
Ma <i>et al.</i> [*] (2023) [71]	statistical-based approach, CNN	CIFAR10, TinyImageNet, CelebA	binary classification
Chang <i>et al.</i> [✱] (2023) [16]	vision-language model (e.g InstructBLIP)	MS COCO, Flickr30k, SD2, SDXL, DeepFloyd IF, DALLE-2, SGXL, ControlNet, SD2-Inpainting, LaMa, SD2-SuperResolution, LTE	visual question answering
Bi-LORA [✱] (Ours)	vision-language model (e.g BLIP2, ViTGP2)	LSUN Bed, ADM, LDM, DDPM, IDDP, PNDM, SD v-1.4, GLIDE	image captioning

^{*} Deep feature. ^{*} Diffusion models unique attribute. [✱] Vision-language models.

applying multiLID to these features, and training a random forest classifier on the multiLID scores.

In [64], a novel approach to detect AI-generated images is introduced. The method employs a cross-attention-enhanced dual-stream network designed to efficiently capture various features of such images, with a specific emphasis on texture. The network architecture consists of two streams: the residual stream, utilizing an spatial rich model (SRM) [72] residual extraction module to capture residual information, and the content stream, focusing on low-frequency aspects of the images.

Furthermore, [63] proposed a distinctive synthetic image detection method named language-guided synthesis detection (LASTED). This approach leverages language-guided contrastive learning and a unique formulation of the detection problem to enhance the extraction of highly discriminative representations from limited data. LASTED augments training images with carefully designed textual labels, enabling joint image-text contrastive learning for forensic feature extraction. Unlike traditional classification-based approaches, this method treats synthetic image detection as an identification problem, offering a unique and effective perspective to address the challenges in synthetic image detection.

Furthermore, a two-branch global and local feature fusion method was proposed in [66] for the detection of AI-synthesized images. This method combines multi-scale global features and informative local features using a ResNet50 [59] backbone network, known for its efficiency and effectiveness in various face-related tasks. The input image is processed by ResNet50, and an attention-based multi-scale feature fusion (AMSFF) module is employed to fuse low-level and high-level features, creating a global representation. This global representation is then fed into a local branch where the patch selection module (PSM) identifies key patches with significant energy and classification relevance. Local features

are extracted from these selected patches and integrated with the global representation using an attention-based module for final binary classification.

In contrast to conventional rule-based techniques [73, 74, 75], Sinita *et al.* [67] introduced a novel rule-based method that achieves high detection accuracy, even when trained with a small set of generative images (fewer than 512). This approach leverages the inductive bias of CNNs to extract distinctive features (fingerprints) from various generators in the training data, enabling the detection of generative images from the same model and its fine-tuned versions.

More recently, Chang *et al.* [16] drew inspiration from the zero-shot capabilities of VLMs and proposed an approach that leverages VLMs such as InstructBLIP. The method incorporates prompt tuning techniques to enhance deepfake detection accuracy over unseen data. The authors reframed the deepfake detection problem as a visual question-answering task, fine-tuning soft prompts for InstructBLIP to distinguish whether a query image is real or fake. On a different note, Cozzolino *et al.* [69] introduced a lightweight detection strategy based on contrastive language image pre-training (CLIP) features. These features are employed to design a linear support vector machine (SVM) classifier, and the proposed strategy is evaluated for its performance in challenging scenarios. Finally, Table I summarizes state-of-the-art models proposed for the synthetic image detection problem.

III. SYNTHETIC IMAGE DETECTION WITH VLMs

In this section, we present our approach for addressing synthetic image detection using large-scale VLMs. Our approach reframes the binary classification task into an image captioning task, leveraging cutting-edge VLMs models (e.g., BLIP2). Fig. 2 provides a visual representation of our methodology built around the bootstrapping language image pre-training (BLIP)2 architecture.

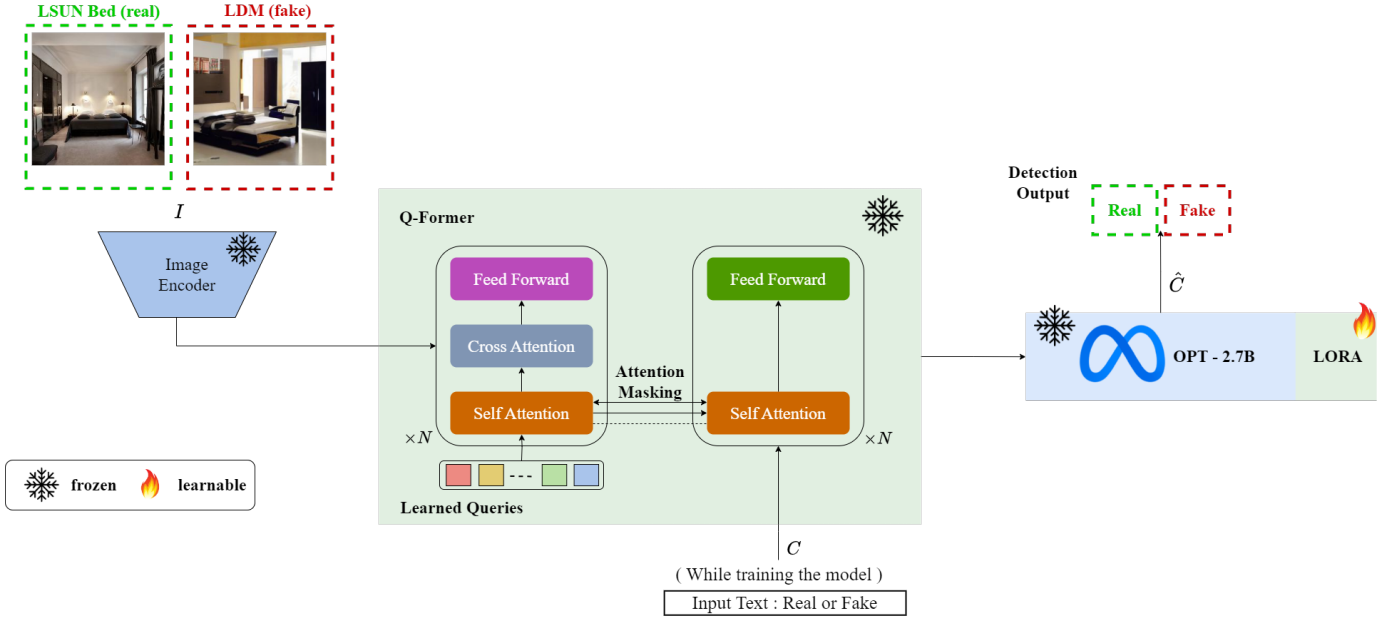


Fig. 2: Bi-LORA finetuning for synthetic image detector.

A. Synthetic Image Detection

Synthetic image detection is generally a binary image classification task. Its main objective is to develop a model \mathcal{M} that learns a function $f : \mathbf{I} \rightarrow \mathbf{Y}$ from the training set $D = \{(I_i, y_i) | 1 \leq i \leq n\}$, where $I_i \in \mathbf{I} = \mathbb{R}^{d \times d}$ is an image, and $y_i \in \mathbf{Y} = \{0, 1\}$ represents the class labels. Here, 0 indicates images captured from the real world, and 1 indicates generated images. The model’s objective is to predict the class \hat{y} for an input image I as follows:

$$\hat{y} = f_{\theta}(I), \quad (1)$$

where \hat{y} is the predicted class label (0 or 1), and θ represents the model parameters.

B. VLM Fine-Tuning for Synthetic Image Detection

In the previous subsection, we introduced synthetic image detection from a general perspective and will now proceed to reframe it as an image captioning problem, harnessing the capabilities of VLMs. Instead of treating synthetic image detection as a traditional binary classification task, we will employ VLMs to generate descriptive captions for each image. The VLMs will learn to produce captions that capture the essence of the image, and these captions will serve as indicators of the image’s authenticity. Specifically, the model will generate captions that fall into one of two categories: “real” or “fake.”

Let’s define this fine-tuning process mathematically. We have a VLM \mathcal{M} with parameters θ , which takes an image I as input and generates a caption \hat{C} . We denote this process as:

$$\hat{C} = \mathcal{M}_{\theta}(I). \quad (2)$$

The caption \hat{C} is a human-like label (textual description) of the image, and it will be used to distinguish the “real” image from the “fake”.

To tune the model for this task, we have a dataset $D = \{(I_i, C_i) | 1 \leq i \leq n\}$, where I_i is the i -th image, and C_i is the ground truth caption whether the image is “real” or “fake”. The model’s objective is to minimize a suitable loss function \mathcal{L} over this dataset:

$$\theta^* = \arg \min_{\theta} \sum_{i=1}^n \mathcal{L}(\mathcal{M}_{\theta}(I_i), C_i). \quad (3)$$

Once fine-tuned, the VLM will be capable of generating captions that help categorizing images into the desired class, providing a more detailed and expressive approach to synthetic image detection. In the following subsections, we will delve into the details of the fine-tuning process of our Bi-LORA method.

C. LORA Tuning Technique

Fine-tuning large pre-trained models is a computational challenge, often involving the adjustment of millions of parameters. This traditional tuning approach, while efficient, requires considerable resources and computational time, creating a bottleneck for the adaptation of these models to specific tasks. LORA [76] presents an effective solution to this problem by decomposing the update matrix during fine-tuning, Fig. 3 (left).

In the traditional fine-tuning method, we modify the weights of a large pre-trained model to adapt it to a new task. This adaptation involves modifying the model’s original weight matrix W . Changes made to W during fine-tuning are collectively represented by ΔW , so the updated weights can be expressed as $W + \Delta W$. Instead of directly modifying W , the LORA approach seeks to decompose ΔW . Such decomposition is a

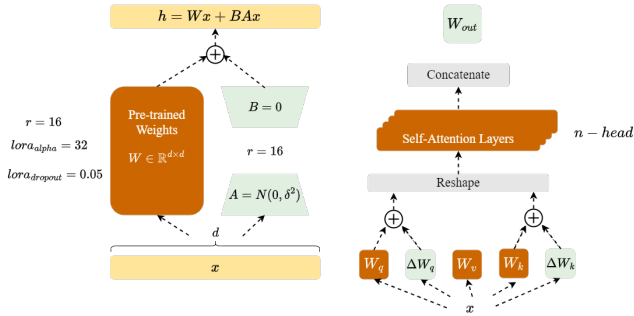


Fig. 3: Bi-LORA fine-tuning with LORA.

crucial step in reducing the computational overhead involved in fine-tuning large models.

Intrinsic rank assumption suggests that significant changes in the large pre-trained model can be captured using a lower-dimensional representation. Fundamentally, it asserts that not all elements of ΔW are equally important; instead, a smaller subset of these changes can effectively capture the necessary adjustments. Thus, based on this assumption, LORA proposes to represent ΔW as the product of two smaller matrices, A and B , with a lower rank. Thus, the updated weight matrix W' becomes:

$$W' = W + \Delta W = W + BA. \quad (4)$$

Here, W remains fixed (i.e. it is not updated during training). B and A are low-dimensional matrices, and their product BA represents a low-rank approximation of ΔW .

Choosing lower-rank matrices A and B via the LORA technique results in a notable decrease in trainable parameters, providing advantages in memory efficiency, faster training, adaptability, hardware compatibility, and scalability for large neural networks during fine-tuning.

D. LORA Tuning on Bi-LORA

BLIP2 [7] is a method that improves vision-language alignment using a querying transformer (Q-Former) as a bridge. Q-Former extracts relevant visual information from frozen image encoders and provides it to a frozen language model. The method undergoes two pre-training phases: one for learning visual representations for text and another for training the Q-Former to provide interpretable visual input to the language model. Thus, the smaller matrices are trained to learn task-specific information using supervised learning. Figure 3 (right) provides a visual overview of fine-tuning the BLIP2 model using the LORA technique. During fine-tuning, we keep the pretrained BLIP2 model weights (W) frozen and inject a pair of trainable rank decomposition matrices (A and B) into each self attention layer, enabling us to optimize and adapt these layers to our new detection task without incurring excessive computational overhead. Thus, the smaller matrices are trained to learn task-specific information using supervised learning. This method is commonly referred to as LORA [76], which

falls under the re-parameterization category of parameter-efficient fine-tuning (PEFT) methods. Specifically, the update of BLIP2 pre-trained weight matrix W is constrained by a low-rank decomposition $W + \Delta W = W + BA$. Note that both W and $\Delta W = BA$ are multiplied by the same input x , and their respective output vectors are summed coordinate-wise. For $h = Wx$, the modified forward pass yields:

$$h = Wx + \Delta Wx = Wx + BAx. \quad (5)$$

It is worth highlighting that, among various attention weights, we adapt only two types: W_q and W_k of the large language model (LLM) decoder module. The first consequence of this technique is that the number of parameters to train is really small, Table II. However, we run into a second, maybe more important consequence, which is that because we don't alter the weights of the pretrained model, it doesn't change its behavior or forget anything it has previously learned, thus we can use it for other tasks if need be.

TABLE II: Number of parameters for each Bi-LORA's module and the number updated with LoRa

Modules	Trainable	Freeze
Query Tokens	0	24,576
Image encoder	0	985,952,256
Qformer	0	105,137,664
Projection Layer	0	1,968,640
LLM (OPT 2.7b)	5,242,880	2,651,596,800
Total	5,242,880	3,744,679,936

Percentage of trainable parameters: 0.14%

IV. EXPERIMENTAL RESULTS

This section discusses the empirical results of our proposed synthetic image detection methodology. We present an overview of the experimental setup, delve into cross-generator evaluations, and assess the model's resilience to adversarial conditions.

A. Experimental Setup

Dataset. To comprehensively evaluate the performance of our proposed method in synthetic image detection, we employed an existing dataset introduced by Ricker *et al.* [3]. This dataset incorporates real images sourced from the large-scale scene understanding (LSUN) bedroom dataset [20]. We curated a collection of images generated by five distinct diffusion models, all trained on LSUN bedroom dataset [20]. Among these models, four subsets of generated images (ADM [21], DDPM [22], iDDPM [23], and PNDM [24]) are generated by unconditional diffusion models. The fifth subset (LDM [25]) is generated by text-to-image diffusion model. Further, for generalization evaluation to text-to-image generation, we expanded the dataset by incorporating two additional models: stable diffusion (SD) [25] and GLIDE [26]. The text prompt used to generate these images was "A photo of a bedroom".

In our experiment, all the subsets consist of 42,000 generated images along with their corresponding real samples from the LSUN bedroom dataset [20]. Each subset is divided

into 40,000 images for training, 1,000 for validation, and 10,000 for testing purposes. It is worth noting that the real images used for testing is consistent across all the testing subsets. Further details regarding the dataset are provided in the GitHub codebase, in Fig. 1, we present a selection of representative examples.

Evaluation metrics. Following the convention of previous detection methods [71] [60] [65], we report the accuracy (ACC) and F1 score (F1-Score) in our experiments. Accuracy (ACC) measures the proportion of correct predictions, with higher scores indicating better performance. While F1-Score balances precision and recall, offering a single measure of a model’s accuracy in identifying positive instances while minimizing false results.

Baselines. To comprehensively evaluate and compare our proposed approach, we tailored several prominent models, namely ResNet50 [17], Xception [18], DeiT [19], and ViTGPT2¹ trained on our dataset, to establish baseline benchmarks. We opted for these models due to their extensive usage and outstanding performance in related tasks. To formulate our baseline models, we fine-tuned these architectures by substituting their final fully-connected (FC) layers with a novel FC layer featuring a single neuron dedicated to discerning the authenticity of images. These models were initialized with pre-trained weights gleaned from the ImageNet dataset [77], thereby harnessing the knowledge encoded in their learned representations. Employing these custom-tailored baselines enables us to assess the efficacy of our proposed approach when compared with well-established and widely-adopted image classification architectures.

Implementation details. In our experiments, we leveraged the PyTorch deep learning framework on a Windows 11 Pro computer equipped with an NVIDIA RTX A4500 GPU with 16 GB and an Intel(R) i9-12950HX CPU. Our study used baseline models obtained from their publicly available repositories, which we fine-tuned to align with our specific experimental setup. For Bi-LORA model tuning, we opted for the Adam [78] optimizer with default settings, a learning rate of $5e-5$, and training epoch of 20 epochs. During training, we configured the PEFT module, in particular LORA, with the followings parameters: a *rank* of 16, *lora_alpha* set to 32, *lora_dropout* at 0.05, and a *batch_size* of 32. Regarding ViTGPT2 model, we followed a procedure outlined by the author, as detailed in provided note¹. To ensure a fair comparison, we retrain all baselines on our training dataset, instead of using their published versions directly.

B. Cross-Generator Synthetic Image Detection

Table III presents the performance metrics of the proposed Bi-LORA model. It was trained on the training set associated with seven generative models and evaluated on their corresponding testing sets. In the table, the diagonal entries reflect the detector’s performance when trained and tested on images generated by the same generator. We observe

that the detector achieves an accuracy exceeding 96.51% when both training and testing are conducted on images generated by the same model. Significantly, the subsets SD (SD V-1.4) and Glide demonstrate precision rates of 100%. Nevertheless, a notable decline in performance is observed when the model is trained and tested with data generated by different generators. For example, when Bi-LORA is trained on the ablated diffusion model (ADM) and improved denoising diffusion probabilistic models (IDDP) subsets and subsequently tested on stable diffusion (SD V-1.4), the precision diminishes to 48.32% and 49.58%, respectively. Conversely, the training subsets of SD (SD V-1.4) and Glide exhibit poor overall generalization. These two models yield an accuracy of approximately 50% across all unconditional diffusion-based models and LDM, indicating their inefficacy in distinguishing AI-generated images from real ones. This inefficiency is further evident in the extremely low F1-Scores of these subsets, suggesting challenges in identifying AI-generated images by unconditional diffusion-based models and LDM. Furthermore, the experiment highlights LDM and pseudo numerical methods for diffusion models on manifolds (PNDM) as the most influential contributors, while SD (SD V-1.4) and Glide exhibit limitations in performance, especially within our bedroom dataset. Moreover, it is noteworthy that when the Bi-LORA model is trained on an unconditional diffusion-based model, it demonstrates robust generalization to other generative models compared to when trained on a text-to-image model, specifically SD (SD V-1.4) and Glide.

In light of this empirical observation, discerning fake generated images from a specific generator may seem like a straightforward task, achieved by training a detector on a dataset containing both authentic and synthesized images. However, it is crucial to acknowledge that this method may have limitations when confronted with generators of unknown provenance. In practical scenarios, the identity of the generator often remains concealed during the training phase. In the context of our research, we aim to rigorously evaluate the generalization prowess of our Bi-LORA, i.e., its ability to distinguish authentic from synthetic images, regardless of the underlying generator. To this end, we introduce the cross-generator synthetic image detection experiment as an effective means of evaluating the detection capability of the AI-generating detector.

From Table III, it is evident that the most favorable outcomes are achieved through training on the LDM. Consequently, we conduct training of the baseline models on LDM and evaluate their performance on test subsets from various generators. The table IV also reports the average accuracy across these diverse test subsets.

In all test subsets, the assessed models exhibited varying levels of accuracy in detecting synthetic images. ResNet50 [59] consistently demonstrated high accuracy, ranging from 72.33% to 88.96%, across all tested subsets. Conversely, Xception [18] exhibited relatively lower performance, with accuracy ranging from 52.05% to 63.84%. DeiT showed an intriguing pattern, achieving an accuracy of 96.02% on the SD v1.4 subset, while its accuracy was notably lower on other subsets, suggesting potential challenges in specific synthetic image detection sce-

TABLE III: Results of cross-validation on different training and testing subsets using Bi-LORA. We report ACC (%) / F1-Score (%) values.

Training Subset	Testing Subset							Average (in %)
	LDM*	ADM [⊕]	DDPM [⊕]	IDDPM [⊕]	PNDM [⊕]	SD*	GLIDE*	
LDM	99.12 / 99.13	85.24 / 82.97	98.47 / 98.47	97.02 / 96.97	99.22 / 99.23	77.68 / 71.79	97.09 / 97.05	93.41 / 92.23
ADM	95.91 / 95.91	96.51 / 96.57	97.24 / 97.31	97.35 / 97.42	96.16 / 96.21	48.32 / 3.35	70.99 / 61.90	86.07 / 78.38
DDPM	97.94 / 97.94	90.49 / 89.76	98.74 / 98.76	98.52 / 98.53	98.64 / 98.66	50.70 / 7.19	74.22 / 66.36	87.04 / 79.60
IDDPM	97.06 / 97.03	94.16 / 93.94	98.72 / 98.74	98.78 / 98.79	98.02 / 98.03	49.58 / 2.74	62.31 / 41.63	85.52 / 75.84
PNDM	96.66 / 96.58	73.82 / 64.96	96.9 / 96.84	91.82 / 91.19	99.52 / 99.53	85.37 / 83.05	97.93 / 97.91	91.72 / 90.01
SD	50.14 / 0.58	50.00 / 0.00	50.00 / 0.00	50.00 / 0.00	51.74 / 6.73	100.00 / 100.00	99.74 / 99.73	64.52 / 29.58
GLIDE	50.72 / 2.88	50.00 / 0.00	50.03 / 0.14	50.0 / 0.02	58.38 / 28.71	93.56 / 93.12	100.00 / 100.00	64.67 / 32.12

* Text-To-Image diffusion-based model. [⊕] Unconditional diffusion-based model.

TABLE IV: Results of different methods trained on LDM and evaluated on different testing subsets. We report ACC (%) / F1-Score (%).

Method	Testing Subset							Average (in %)
	LDM*	ADM [⊕]	DDPM [⊕]	IDDPM [⊕]	PNDM [⊕]	SD v1.4*	GLIDE*	
ResNet50	99.92 / 99.92	72.33 / 61.83	75.26 / 67.21	88.96 / 87.61	77.20 / 70.52	75.47 / 67.57	73.10 / 63.28	80.32 / 73.99
Xception	99.96 / 99.96	52.05 / 7.98	58.60 / 29.41	54.62 / 16.99	60.01 / 33.43	63.84 / 43.41	58.92 / 30.35	64.00 / 37.36
DeiT	99.83 / 99.83	50.40 / 2.01	50.18 / 1.17	50.14 / 1.01	56.25 / 22.54	96.02 / 95.86	98.15 / 98.11	71.56 / 45.79
ViTGPT2	99.40 / 99.40	70.84 / 59.21	69.60 / 56.72	84.08 / 81.20	95.40 / 95.22	99.54 / 99.55	99.27 / 99.27	88.30 / 84.37
Bi-LORA	99.12 / 99.13	85.24 / 82.97	98.47 / 98.47	97.02 / 96.97	99.22 / 99.23	77.68 / 71.79	97.09 / 97.05	93.41 / 92.23

* Text-To-Image diffusion-based model. [⊕] Unconditional diffusion-based model.

TABLE V: Results of cross-validation on different training and test subsets using different models. Five models trained on seven generators are tested on one generator, and their average accuracy is each data point in the testing subset column. We report ACC (%) / F1-Score (%).

Method	Testing Subset							Average (in %)
	LDM*	ADM [⊕]	DDPM [⊕]	IDDPM [⊕]	PNDM [⊕]	SD v1.4*	GLIDE*	
ResNet50	75.72 / 54.28	69.34 / 43.50	61.23 / 25.83	76.83 / 55.22	61.87 / 27.58	77.18 / 60.40	82.17 / 68.88	72.04 / 47.96
Xception	77.16 / 58.65	69.50 / 41.73	72.13 / 46.72	71.80 / 45.16	64.66 / 37.00	74.09 / 54.21	85.58 / 79.23	73.56 / 51.82
DeiT	71.17 / 48.49	69.52 / 41.05	57.29 / 15.98	70.94 / 42.56	62.37 / 31.07	72.79 / 55.70	86.93 / 82.63	70.14 / 45.35
ViTGPT2	77.43 / 60.86	67.92 / 44.73	74.57 / 56.54	78.17 / 61.70	84.10 / 69.84	76.80 / 60.89	89.35 / 87.38	78.33 / 63.13
Bi-LORA	83.94 / 70.01	77.17 / 61.17	84.30 / 70.04	83.35 / 68.99	85.95 / 75.30	72.17 / 51.61	86.04 / 80.65	81.85 / 68.25

* Text-To-Image diffusion-based model. [⊕] Unconditional diffusion-based model.

narios. Specifically, DeiT performed well in the context of text-to-image generative models (i.e., LDM, SD v1.4, GLIDE), indicating robust generalization to unseen models from the same subcategory used during training. ViTGPT2 delivered competitive results, with accuracy rates ranging from 69.60% to an impressive 99.54%. Notably, Bi-LORA emerged as a standout performer, showcasing outstanding accuracy rates across all subsets, ranging from 77.68% to 99.22%. This underscores its robustness in detecting various types of synthetic content.

In Table V, for each model, we have trained seven versions, one for each of the seven generators. We evaluated each version on seven generator test subsets. We calculated the average over seven results for a given model. For example, we respectively trained seven Bi-LORA models using seven generators and calculated the average of their evaluation results on LDM, resulting in the highest accuracy of 83.94%. Our experiment of detecting synthetic images across different generators reveals valuable information about the robustness and

limitations of the models evaluated. While some models show solid performance when trained and tested on images from the same generator, challenges emerge in scenarios where identity of the generator is unknown during training. Notably, Bi-LORA stands out as an outstanding performer, demonstrating remarkable accuracy across various generator models.

C. Degraded Synthetic Image Detection

In the context of image transmission, images often undergo degradation artifacts due to downscaling to low resolution, compression, and noise interference. Detectors are expected to demonstrate robustness to these distortions. To address this concern, we propose evaluating detectors' performance on degraded images, which more accurately simulate practical conditions, as outlined in Table VI. After training the detectors on the LDM subset, we employ various methods to degrade only the test set images. Specifically, we reduce the image resolution to 112 pixels, employing a scaling factor of 2X. Additionally, we apply JPEG compression with quality settings

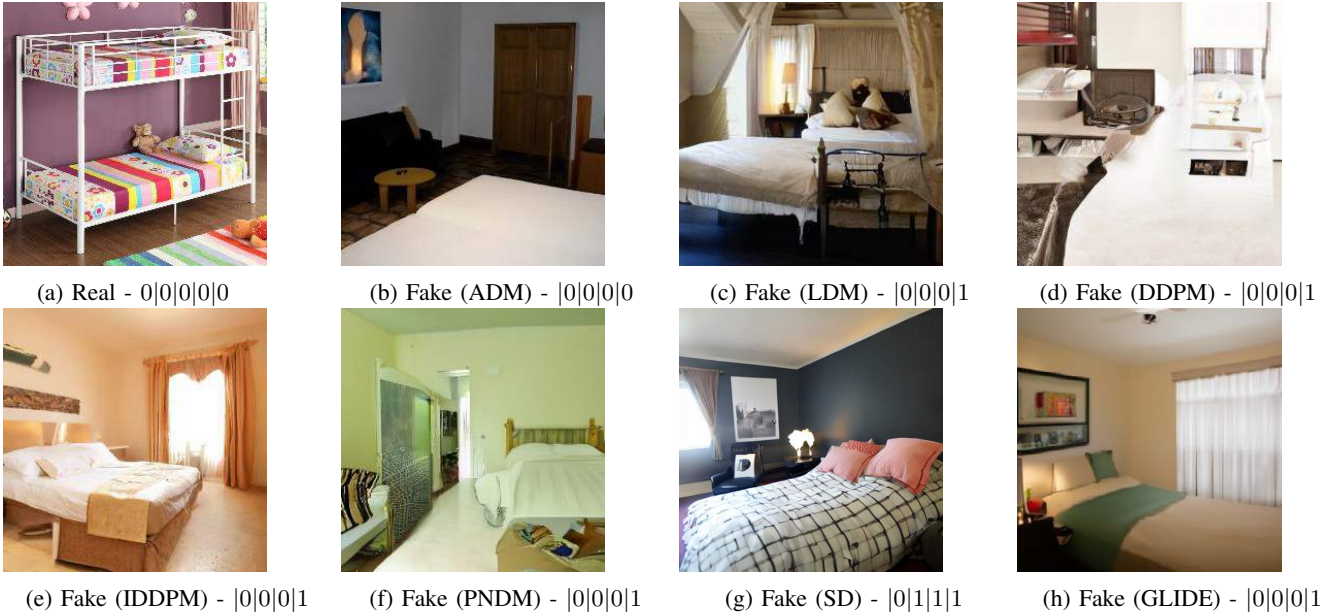


Fig. 4: Each sub-figure represents a random compressed (JPEG $q=65$) image from a testing set, with predicted labels provided below. The 5-digit binary code shows results from ResNet, Xception, DeiT, ViTGP2, and Bi-LORA models, where '0' means real and '1' means fake. It is important to note that all generated images are considered fake.

of 65, introducing compression artifacts. To simulate blurring effects, we apply Gaussian blur with a standard deviation of 3, denoted as $\sigma = 3$.

Consequently, the development of a well-thought-out pre-processing approach holds great promise in addressing the challenge of detecting degraded images. Assessing these detectors on degraded images provides valuable insights into their performance under various challenging conditions. This evaluation contributes to a more comprehensive understanding of the detector's capability to handle practical image degradation.

TABLE VI: Models evaluation on degraded images. LR denotes Low Resolution, q denotes quality.

		Method	ResNet50	Xception	DeiT	ViTGP2	Bi-LORA
Testing Subset	LDM	LR (112)	82.56 / 81.93	61.40 / 67.12	98.42 / 98.44	93.16 / 93.6	95.65 / 95.77
		JPEG ($q=65$)	95.79 / 95.96	50.11 / 0.44	50.00 / 0.00	54.58 / 16.95	90.77 / 89.85
		Blur ($\sigma = 3$)	51.36 / 5.57	69.56 / 73.61	58.88 / 70.77	76.65 / 80.83	85.36 / 87.08
	ADM	LR (112)	68.74 / 62.22	56.77 / 61.65	53.99 / 18.78	85.17 / 84.99	89.14 / 88.74
		JPEG ($q=65$)	73.37 / 67.41	50.02 / 0.08	50.00 / 0.00	50.6 / 2.56	69.38 / 56.00
		Blur ($\sigma = 3$)	50.38 / 1.76	63.20 / 66.24	57.20 / 69.21	68.58 / 72.37	80.53 / 82.07
	DDPM	LR (112)	76.98 / 74.69	58.62 / 63.89	54.36 / 19.96	88.93 / 89.20	96.16 / 96.28
		JPEG ($q=65$)	90.5 / 90.39	50.02 / 0.06	50.04 / 0.14	52.33 / 9.08	93.16 / 92.67
		Blur ($\sigma = 3$)	51.50 / 6.08	65.82 / 69.37	56.28 / 68.33	74.24 / 78.42	85.60 / 87.34
	IDDPM	LR (112)	78.05 / 76.15	61.57 / 67.30	52.52 / 13.94	90.66 / 91.05	95.88 / 96.01
		JPEG ($q=65$)	87.77 / 87.27	50.04 / 0.18	50.01 / 0.04	52.00 / 7.89	88.16 / 86.60
		Blur ($\sigma = 3$)	51.10 / 4.55	67.58 / 71.41	56.74 / 68.78	73.91 / 78.08	85.37 / 87.07
PNDM	LR (112)	78.92 / 77.32	57.03 / 61.96	68.06 / 54.84	92.76 / 93.19	96.27 / 96.39	
	JPEG ($q=65$)	89.99 / 89.82	50.02 / 0.10	50.00 / 0.00	53.44 / 13.05	97.0 / 96.91	
	Blur ($\sigma = 3$)	51.15 / 4.78	69.4 / 73.43	58.30 / 70.24	76.28 / 80.46	85.76 / 87.49	
SD v1.4	LR (112)	72.80 / 68.66	61.68 / 67.42	93.25 / 92.96	93.18 / 93.61	88.10 / 87.49	
	JPEG ($q=65$)	62.72 / 47.53	74.40 / 65.59	95.72 / 95.53	85.06 / 82.45	86.26 / 84.10	
	Blur ($\sigma = 3$)	51.94 / 7.72	77.09 / 81.36	54.12 / 66.24	76.87 / 81.04	71.14 / 70.87	
GLIDE	LR (112)	79.36 / 77.89	66.84 / 73.00	96.88 / 96.87	93.06 / 93.49	93.98 / 94.04	
	JPEG ($q=65$)	89.09 / 88.80	50.90 / 3.52	50.00 / 0.00	57.03 / 24.79	98.39 / 98.37	
	Blur ($\sigma = 3$)	50.94 / 3.95	69.57 / 73.62	59.01 / 70.89	72.31 / 76.42	83.06 / 84.76	

Table VI presents the evaluation results for different models

on degraded images. ResNet50 demonstrates varying performance across different degradation methods, notably excelling under JPEG compression, due to being trained on data that has been compressed with settings ranging from 60 to 100. Conversely, Bi-LORA exhibits robust performance across all degradation methods, highlighting its effectiveness in handling challenges associated with detecting degraded synthetic images. These results underscore the significance of evaluating detectors under challenging conditions to assess their practical suitability in real-world scenarios and emphasize the necessity for models that can reliably perform in the presence of image degradation.

Fig. 4 presents visual examples of randomly selected compressed (JPEG $q=65$) images from testing sets, with predicted labels below each image. The visual examples highlight the challenges posed by image degradation on detection models. In some cases, the models exhibit accurate predictions even in the presence of degradation, while in others, degradation introduces ambiguity, leading to misclassifications. Once again, Bi-LORA consistently demonstrates robust performance across various degradation methods, showcasing its effectiveness in handling challenges related to detecting degraded synthetic images. These visual examples complement the quantitative results presented in Table VI, providing a more intuitive understanding of how different models respond to degraded images. The variability in performance across models and degradation methods underscores the importance of comprehensive evaluations under realistic conditions to assess the practical suitability of image detection models.

D. Generalization to GAN models

In this section, our aim is to investigate whether our Bi-LORA approach, primarily tuned for detecting images gen-

TABLE VII: Evaluation of seven trained Bi-LORA models on five GAN-based testing subsets. We report ACC (%) / F1-Score (%).

Training Subset	Testing Subset					Average (in %)
	StyleGAN	Diff-StyleGAN2	Diff-ProjectedGAN	ProGAN	ProjectedGAN	
LDM	99.09 / 99.09	99.10 / 99.10	99.08 / 99.08	99.26 / 99.26	99.23 / 99.23	99.15 / 99.15
ADM	85.92 / 84.54	90.93 / 90.56	96.56 / 96.74	97.30 / 97.37	96.52 / 96.58	93.47 / 93.16
DDPM	93.80 / 93.56	96.24 / 96.19	98.31 / 98.32	98.80 / 98.81	98.43 / 98.45	97.12 / 97.07
IDDPM	89.67 / 88.76	93.64 / 93.37	97.78 / 97.78	98.74 / 98.75	97.70 / 97.70	95.51 / 95.27
PNDM	99.15 / 99.15	99.44 / 99.45	98.60 / 98.59	99.56 / 99.57	99.13 / 99.13	99.18 / 99.18
SD	66.06 / 48.62	76.40 / 69.11	51.12 / 4.38	63.91 / 43.53	51.43 / 5.56	61.78 / 34.24
GLIDE	65.36 / 47.02	83.45 / 80.17	57.42 / 25.86	84.42 / 81.54	59.81 / 32.82	70.09 / 53.48
Average (in %)	85.59 / 80.11	91.31 / 89.71	85.55 / 74.39	91.71 / 88.40	86.04 / 75.64	88.04 / 81.65

erated by diffusion-based models, can effectively generalize to GAN-generated images without the need for additional fine-tuning on GAN-specific data. One of the key objectives in assessing the generalization of our Bi-LORA approach to GAN-generated images is to explore the transferability of learned features. Our Bi-LORA approach has acquired knowledge about common features and artifacts present in AI-generated images, particularly those created using diffusion-based models. We hypothesize that some of these features may be transferable and applicable to GAN-generated images. To conduct this analysis, we curated a dataset consisting of various models based on GAN, including Diff-StyleGAN2 [79], Diff-ProjectedGAN [79], ProGAN [30], ProjectedGAN [80], and StyleGAN [31]. Each of these subsets comprises 10,000 generated images along with 10,000 real samples. Our approach involves using this dataset to evaluate the performance of our fine-tuned Bi-LORA approach in distinguishing images generated by GAN from real images.

In Table VII, we present the performance evaluation of seven trained Bi-LORA models across five testing subsets based on GANs. Notably, models such as LDM, ADM, denoising diffusion probabilistic models (DDPM), IDDPM, and PNDM consistently exhibit high accuracy and F1-scores. This suggests that our Bi-LORA approach trained on diffusion-based models generalize effectively to images generated by GANs. The remarkable consistency in performance across different GAN models indicates that Bi-LORA have successfully learned features and patterns that are transferable between diffusion-based and GAN-based generative models.

However, StyleGAN presents a challenge, particularly for Bi-LORA model trained on SD and GLIDE generators, where both accuracy and F1-score are considerably lower compared to other GAN models. This discrepancy may be attributed to the unique architecture and characteristics of StyleGAN, requiring specific features that were not as prominent in diffusion-based models. Bi-LORA trained on different generators exhibits varied performance on GAN models. For instance, PNDM consistently performs well across all GAN subsets, while SD and GLIDE show lower performance, indicating differences in feature importance and generalization capabilities among these models.

The findings suggest that our Bi-LORA approach trained on diffusion-based models can generalize to GAN-generated images to a considerable extent. This has implications for applications where detecting AI-generated content is crucial,

such as content moderation and deepfake detection.

E. Comparative Analysis of Synthetic Image Detection Models

In this section, we perform a comparative analysis of Bi-LORA against four recent synthetic image detection models : **AntifakePrompt** (Chang *et al.*, 2023) [16], **DE-FAKE** (Sha *et al.*, 2022) [58], **UniversalFakeDetect** (Ojha *et al.*, 2023) [81], **CNNDetection** (Wang *et al.*, 2020) [82]. For AntifakePrompt, we use checkpoints of detector trained on MS COCO vs. SD2 and MS COCO vs. SD2+LaMa. For DE-FAKE, we employ the checkpoint of the hybrid detector, which considers both the image and the corresponding prompts in inference time. For CNNDetection and UniversalFakeDetect, we use the detectors checkpoint trained on a dataset containing images that may have undergone Gaussian blurring and JPEG augmentation, each with a probability of 10%.

Table VIII compares the performance of four state-of-the-art (SOTA) models on the task of synthetic image detection. It shows the average accuracy of each model on various test datasets (ADM,DDPM etc.) when trained on different real vs. fake image set combinations (e.g., MS COCO vs. SD2+LaMa). The performance of all models varies depending on the training data used. For example, UniversalFakeDetect and CNNDetection perform exceptionally well on the LSUN Bed test set, but perform poorly on other testing sets. In addition, some test data sets seem to be more challenging than others. For instance, AntifakePrompt, Bi-LORA, CNNDetection and UniversalFakeDetect struggle on the SD v1.4 dataset, suggesting that these models may have difficulty detecting certain types of synthetic images.

AntifakePrompt achieves the highest accuracy on the GLIDE and ADM test set. However, performance drops significantly on the datasets generated by the other models when trained on MS COCO vs. SD2. In contrast, it generalizes quite well on the test sets when trained on the MS COCO vs. SD2+LaMa combination.

Regarding the DE-FAKE detector, trained on images generated by SD and MS COCO, it achieves the highest accuracy on the SD v1.4 test set, however it suffers from drops in accuracy when applied to images generated by unseen generative models. Although the model considers corresponding prompts, potentially helping to detect unusual synthetic scenarios, its effectiveness is limited because most of the training data uses natural prompts from the MS COCO dataset. This biases

TABLE VIII: Comparison with SOTA models

Methods	Training Set	LSUN Bed	ADM	DDPM	IDDPM	PNDM	LDM	SD v1.4	GLIDE
AntifakePrompt	MS COCO vs. SD2	92.86	29.76	57.05	47.99	76.79	57.21	5.80	98.86
	MS COCO vs. SD2+LaMa	65.58	73.18	87.59	82.33	92.31	88.56	6.80	99.62
DE-FAKE	MS COCO vs. SD2	27.87	42.70	55.95	31.69	44.24	53.43	80.95	49.90
UniversalFakeDetect	LSUN vs. ProGAN	99.80	06.80	36.10	24.70	47.50	34.10	21.70	12.00
CNNDetection	LSUN vs. ProGAN	99.80	00.90	01.67	01.46	01.46	01.30	02.62	07.92
Bi-LORA (Ours)	LSUN Bed vs. LDM	98.55	71.93	98.39	95.49	99.89	99.70	56.81	95.63

TABLE IX: General Image Datasets

Dataset	#Real	#Generated	Source of Real Image	Generation Method	Year
Synthbuster	-	9,000	Raise-1k	DALL-E2&3, Midjourney, SDMs, GLIDE, Firefly	2023
GenImage	1, 331,167	1,350,000	ImagNet	SDMs, Midjourney, BigGAN	2023
CIFAKE	60,000	60,000	CIFAR-10	SD v1.4	2023
AutoSplice	2,273	3,621	Visual News	DALL-E 2	2023
DiffusionDB	3,300,000	16,000,000	DiscordChatExporter	SD	2023
ArtiFact	964,989	1,531,749	COCO, FFHQ, LSUN	SDMs, DDPM, LDM, CIPS	2023
HiFi-IFDL	~600,000	1,300,000	FFHQ, COCO, LSUN	DDPM, GLIDE, LDM, GANs	2023
DiffForensics	232,000	232,000	LSUN, ImageNet	LDM, DDPM, VQDM, ADM	2023
CocoGlide	512	512	COCO	GLIDE	2023
LSUNDB	420,000	510,000	LSUN	LDM, ADM, DDPM, IDDPM, PNDM, StyleGAN, ProGAN, Diff-ProjectedGAN, ProjectedGAN, Diff-StyleGAN2	2023
UniFake	8,000	8,000	LAIION-400M	LDM, GLIDE	2023
REGM	-	116,000	CelebA, LSUN	116 publicly available GMs	2023
DMimage	200,000	200,000	COOC, LSUN	LDM	2022
AIGCD	360,000	508,500	LSUN, COCO, FFHQ	SDMs, GANs, ADM, DALL-E 2, GLIDE	2023
DIF	84,300	84,300	LAION-5B	SDMs, DALL-E 2, GLIDE, GANs	2023
Fake2M	-	2,300,000	CC3M	SD-V1.5, IF, StyleGAN3	2023

the model towards identifying false images, making it less effective against fakes generated with different prompts.

UniversalFakeDetect and CNNDetection, both trained on the LSUN vs ProGAN dataset, show outstanding performance (near-perfect accuracy) on LSUN Bed. Meanwhile, their performance suffers significantly on all other datasets, highlighting a major weakness in terms of generalizability and dependence on a particular training data configuration.

Bi-LORA achieves good accuracy on the majority of test sets (Lsun Bed, DDPM, IDDPM, PNDM, LDM) except SD v1.4, suggesting that Bi-LORA is effective in generalizing to different types of synthetic images.

F. Evaluation on Diverse Datasets

The performance of deep learning models in real-world applications depends not only on their effectiveness in the domains on which they were initially trained, but also on their ability to generalize and adapt to diverse and new data sources. In the context of image authenticity assessment, where it is crucial to distinguish synthetic from real-world images, evaluation on diverse datasets becomes an essential aspect of model validation. In this section, we dive into a comprehensive exploration of the generalizability and robustness of our proposed approach.

Our vision language model, preliminarily fine-tuned on the LSUN bedroom dataset, seems initially specialized in a specific task: distinguishing synthetic bedroom scenes from real ones. While this specialization has yielded promising results in its niche, the wider landscape of visual data extends

far beyond the confines of bedrooms, Table. IX. In real-world applications, the need to detect image authenticity often arises in scenarios where images encompass a myriad of content, with diverse objects, scenes, and contexts. It is therefore imperative to evaluate the performance of our model when applied to more general datasets.

To this end, we are conducting a comprehensive evaluation of our approach on another distinct dataset, presenting different challenges and characteristics. The data set selected for this evaluation has been chosen to represent varying degrees of divergence from the LSUN bedroom dataset, ensuring a rigorous examination of the versatility and adaptability of our approach.

Table X presents the performance of two leading methods, AntifakePrompt and Bi-LORA, on a variety of data sets. These datasets encompass a variety of domains, including image captions (MS COCO), social media (Flickr), synthetic images from text-image generators (SD2, SDXL, IF, DALLE-2, SGXL), image stylization (ControlNet), image inpainting (LaMa, SD2-Inpainting), super-resolution (LTE, SD2-SuperResolution), as well as deep forensic analysis and attack scenarios (Deeper Forensics, Adversarial (Adver.), backdoor attacks, and data poisoning).

AntifakePrompt and Bi-LORA were trained on different sets of data and evaluated on these diverse data sets. The results highlight their effectiveness in the synthetic image detection task. Notably, both methods achieve competitive performance on most data sets, demonstrating their adaptability in real-world applications. Analyzing the table, it's evident that AntifakePrompt consistently achieves high accuracy across

TABLE X: Performance comparison of Bi-LORA trained on a general dataset vs. AntifakePrompt. Experiments are conducted on 2 real and 14 fake datasets, including 3 attacked ones.

Methods	Training Set	No. of param	MS COCO	Flickr	SD2	SDXL	IF	DALLE-2
AntifakePrompt	MS COCO vs. SD2	4.86K	95.37	91.00	97.83	97.27	89.73	99.57
	MS COCO vs. SD2+LaMa	4.86K	90.83	81.04	97.10	97.10	88.37	99.07
Bi-LORA	MS COCO vs. SD2	5.24M	92.10	90.33	99.40	98.30	90.60	99.23
	MS COCO vs. SD2+LaMa	5.24M	80.30	72.53	99.47	99.37	95.03	99.67

Methods	Training Set	No. of param	SGXL	ControlNet	Inpainting		Super Res.	
					LaMa	SD2	LTE	SD2
AntifakePrompt	MS COCO vs. SD2	4.86K	99.97	91.47	39.03	85.20	99.90	99.93
	MS COCO vs. SD2+LaMa	4.86K	99.93	93.27	58.53	90.70	100.00	99.97
Bi-LORA	MS COCO vs. SD2	5.24M	96.80	96.87	46.47	92.30	98.33	99.73
	MS COCO vs. SD2+LaMa	5.24M	98.50	98.90	80.07	94.13	99.67	100.00

Methods	Training Set	No. of param	Deeper-Forensics	Adver.	Attack		Average
					Backdoor	Data Poisoning	
AntifakePrompt	MS COCO vs. SD2	4.86K	97.90	96.70	93.00	91.57	91.59
	MS COCO vs. SD2+LaMa	4.86K	97.77	97.20	97.10	93.63	92.60
Bi-LORA	MS COCO vs. SD2	5.24M	81.67	34.37	47.33	33.00	81.05
	MS COCO vs. SD2+LaMa	5.24M	87.37	88.50	89.73	74.23	91.09

several data sets, particularly when trained on MS COCO vs SD2+LaMa. This indicates its robustness in handling diverse data distributions and adversarial scenarios. On the other hand, Bi-LORA exhibits slightly lower performance in some cases, but still maintains strong results across various data sets.

Moreover, the comparison between training on different datasets (e.g., MS COCO vs. SD2) provides valuable insights into the impact of training data composition on model performance. For example, training on a combination of MS COCO and SD2+LaMa data leads to improved performance in most cases, highlighting the importance of incorporating diverse training data to improve model robustness.

V. CONCLUSION

In this paper, we introduced Bi-LORA, a novel approach to synthetic image detection in response to advancements in realistic image generation. We reconceptualized binary classification as an image captioning task, leveraging the powerful convergence between vision and language, as well as the zero-shot nature of VLMs. Obtained results demonstrated a remarkable average accuracy of **93.41%** in the detection of synthetic image, underling the relevance and effectiveness of Bi-LORA approach to the challenges posed by images generated by unknown generative models. Moreover, unlike previous studies that require millions of parameters to be tuned/learned, Bi-LORA model only needs to adjust far fewer parameters, thus setting a better balance between training cost and efficiency.

Future research could be conducted on the possibility of distilling the mixture of knowledge from very large VLMs to a lightweight model, given that our experimental results highlight the complementarity between Bi-LORA and VitGPT2, considering that VLMs require significant computational and memory resources. Moreover, we aim to take a step further beyond just detecting synthetic images from real ones by attributing them to their source generator using VLMs in

a multitask single-step approach, thereby holding generators accountable for their actions in today’s rapidly evolving technological landscape.

To support the principle of reproducible research and to enable future extensions, we make the code and models publicly available at <https://github.com/Mamadou-Keita/VLM-DETECT>.

ACKNOWLEDGMENTS

This work has been funded by the project PCI2022-134990-2 (MARTINI) of the CHISTERA IV Cofund 2021 program.

REFERENCES

- [1] Z. Lu, D. Huang, L. Bai, X. Liu, J. Qu, and W. Ouyang, “Seeing is not always believing: A quantitative study on human perception of ai-generated images,” *arXiv preprint arXiv:2304.13023*, 2023.
- [2] D. P. Kingma and M. Welling, “Auto-encoding variational bayes,” *arXiv preprint arXiv:1312.6114*, 2013.
- [3] J. Ricker, S. Damm, T. Holz, and A. Fischer, “Towards the detection of diffusion model deepfakes,” *arXiv preprint arXiv:2210.14571*, 2022.
- [4] C. Schuhmann, R. Vencu, R. Beaumont, R. Kaczmarczyk, C. Mullis, A. Katta, T. Coombes, J. Jitsev, and A. Komatsuzaki, “Laion-400m: Open dataset of clip-filtered 400 million image-text pairs,” *arXiv preprint arXiv:2111.02114*, 2021.
- [5] A. Radford, J. W. Kim, C. Hallacy, A. Ramesh, G. Goh, S. Agarwal, G. Sastry, A. Askell, P. Mishkin, J. Clark *et al.*, “Learning transferable visual models from natural language supervision,” in *International conference on machine learning*. PMLR, 2021, pp. 8748–8763.
- [6] J.-B. Alayrac, J. Donahue, P. Luc, A. Miech, I. Barr, Y. Hasson, K. Lenc, A. Mensch, K. Millican, M. Reynolds *et al.*, “Flamingo: a visual language model

- for few-shot learning,” *Advances in Neural Information Processing Systems*, vol. 35, pp. 23 716–23 736, 2022.
- [7] J. Li, D. Li, S. Savarese, and S. Hoi, “Blip-2: Bootstrapping language-image pre-training with frozen image encoders and large language models,” *arXiv preprint arXiv:2301.12597*, 2023.
- [8] A. Singh, R. Hu, V. Goswami, G. Couairon, W. Galuba, M. Rohrbach, and D. Kiela, “Flava: A foundational language and vision alignment model,” in *Proceedings of the IEEE/CVF Conference on Computer Vision and Pattern Recognition*, 2022, pp. 15 638–15 650.
- [9] H. Liu, C. Li, Q. Wu, and Y. J. Lee, “Visual instruction tuning,” *arXiv preprint arXiv:2304.08485*, 2023.
- [10] Z. Wang, J. Yu, A. W. Yu, Z. Dai, Y. Tsvetkov, and Y. Cao, “Simvlm: Simple visual language model pretraining with weak supervision,” *arXiv preprint arXiv:2108.10904*, 2021.
- [11] L. H. Li, M. Yatskar, D. Yin, C.-J. Hsieh, and K.-W. Chang, “Visualbert: A simple and performant baseline for vision and language,” *arXiv preprint arXiv:1908.03557*, 2019.
- [12] W. Dai, J. Li, D. Li, A. Tiong, J. Zhao, W. Wang, B. Li, P. Fung, and S. Hoi, “Instructblip: Towards general-purpose vision-language models with instruction tuning. arxiv 2023,” *arXiv preprint arXiv:2305.06500*, 2023.
- [13] S. Antol, A. Agrawal, J. Lu, M. Mitchell, D. Batra, C. L. Zitnick, and D. Parikh, “Vqa: Visual question answering,” in *Proceedings of the IEEE international conference on computer vision*, 2015, pp. 2425–2433.
- [14] O. Vinyals, A. Toshev, S. Bengio, and D. Erhan, “Show and tell: A neural image caption generator,” in *Proceedings of the IEEE conference on computer vision and pattern recognition*, 2015, pp. 3156–3164.
- [15] K. O’Shea and R. Nash, “An introduction to convolutional neural networks,” *arXiv preprint arXiv:1511.08458*, 2015.
- [16] Y.-M. Chang, C. Yeh, W.-C. Chiu, and N. Yu, “Antifakeprompt: Prompt-tuned vision-language models are fake image detectors,” *arXiv preprint arXiv:2310.17419*, 2023.
- [17] K. He, X. Zhang, S. Ren, and J. Sun, “Deep residual learning for image recognition,” 2015.
- [18] F. Chollet, “Xception: Deep learning with depthwise separable convolutions,” in *Proceedings of the IEEE Conference on Computer Vision and Pattern Recognition (CVPR)*, July 2017.
- [19] H. Touvron, M. Cord, M. Douze, F. Massa, A. Sablayrolles, and H. Jégou, “Training data-efficient image transformers & distillation through attention,” 2021.
- [20] F. Yu, A. Seff, Y. Zhang, S. Song, T. Funkhouser, and J. Xiao, “Lsun: Construction of a large-scale image dataset using deep learning with humans in the loop,” *arXiv preprint arXiv:1506.03365*, 2015.
- [21] P. Dhariwal and A. Nichol, “Diffusion models beat gans on image synthesis,” *Advances in neural information processing systems*, vol. 34, pp. 8780–8794, 2021.
- [22] J. Ho, A. Jain, and P. Abbeel, “Denoising diffusion probabilistic models,” *Advances in neural information processing systems*, vol. 33, pp. 6840–6851, 2020.
- [23] A. Q. Nichol and P. Dhariwal, “Improved denoising diffusion probabilistic models,” in *International Conference on Machine Learning*. PMLR, 2021, pp. 8162–8171.
- [24] L. Liu, Y. Ren, Z. Lin, and Z. Zhao, “Pseudo numerical methods for diffusion models on manifolds,” *arXiv preprint arXiv:2202.09778*, 2022.
- [25] R. Rombach, A. Blattmann, D. Lorenz, P. Esser, and B. Ommer, “High-resolution image synthesis with latent diffusion models,” in *Proceedings of the IEEE/CVF conference on computer vision and pattern recognition*, 2022, pp. 10 684–10 695.
- [26] A. Nichol, P. Dhariwal, A. Ramesh, P. Shyam, P. Mishkin, B. McGrew, I. Sutskever, and M. Chen, “Glide: Towards photorealistic image generation and editing with text-guided diffusion models,” *arXiv preprint arXiv:2112.10741*, 2021.
- [27] J. Betker, G. Goh, L. Jing, T. Brooks, J. Wang, L. Li, L. Ouyang, J. Zhuang, J. Lee, Y. Guo *et al.*, “Improving image generation with better captions,” *Computer Science*. <https://cdn.openai.com/papers/dall-e-3.pdf>, 2023.
- [28] I. Goodfellow, J. Pouget-Abadie, M. Mirza, B. Xu, D. Warde-Farley, S. Ozair, A. Courville, and Y. Bengio, “Generative adversarial nets,” *Advances in neural information processing systems*, vol. 27, 2014.
- [29] A. Radford, L. Metz, and S. Chintala, “Unsupervised representation learning with deep convolutional generative adversarial networks,” *arXiv preprint arXiv:1511.06434*, 2015.
- [30] T. Karras, T. Aila, S. Laine, and J. Lehtinen, “Progressive growing of gans for improved quality, stability, and variation,” *arXiv preprint arXiv:1710.10196*, 2017.
- [31] T. Karras, S. Laine, and T. Aila, “A style-based generator architecture for generative adversarial networks,” in *Proceedings of the IEEE/CVF conference on computer vision and pattern recognition*, 2019, pp. 4401–4410.
- [32] F. Mokhayeri, K. Kamali, and E. Granger, “Cross-domain face synthesis using a controllable gan,” in *Proceedings of the IEEE/CVF winter conference on applications of computer vision*, 2020, pp. 252–260.
- [33] N. Ruiz, B.-J. Theobald, A. Ranjan, A. H. Abdelaziz, and N. Apostoloff, “Morphgan: One-shot face synthesis gan for detecting recognition bias,” *arXiv preprint arXiv:2012.05225*, 2020.
- [34] H. Liz-López, M. Keita, A. Taleb-Ahmed, A. Hadid, J. Huertas-Tato, and D. Camacho, “Generation and detection of manipulated multimodal audiovisual content: Advances, trends and open challenges,” *Information Fusion*, vol. 103, p. 102103, 2024.
- [35] W. Xu, C. Long, R. Wang, and G. Wang, “Drb-gan: A dynamic resblock generative adversarial network for artistic style transfer,” in *Proceedings of the IEEE/CVF international conference on computer vision*, 2021, pp. 6383–6392.
- [36] Y. Chen, Y.-K. Lai, and Y.-J. Liu, “Cartoongan: Generative adversarial networks for photo cartoonization,” in *Proceedings of the IEEE conference on computer vision and pattern recognition*, 2018, pp. 9465–9474.

- [37] S. Yang, Z. Wang, Z. Wang, N. Xu, J. Liu, and Z. Guo, "Controllable artistic text style transfer via shape-matching gan," in *Proceedings of the IEEE/CVF International Conference on Computer Vision*, 2019, pp. 4442–4451.
- [38] X. Zhu, L. Zhang, L. Zhang, X. Liu, Y. Shen, and S. Zhao, "Gan-based image super-resolution with a novel quality loss," *Mathematical Problems in Engineering*, vol. 2020, pp. 1–12, 2020.
- [39] C. Ledig, L. Theis, F. Huszár, J. Caballero, A. Cunningham, A. Acosta, A. Aitken, A. Tejani, J. Totz, Z. Wang *et al.*, "Photo-realistic single image super-resolution using a generative adversarial network," in *Proceedings of the IEEE conference on computer vision and pattern recognition*, 2017, pp. 4681–4690.
- [40] M. S. Sajjadi, B. Scholkopf, and M. Hirsch, "Enhancenet: Single image super-resolution through automated texture synthesis," in *Proceedings of the IEEE international conference on computer vision*, 2017, pp. 4491–4500.
- [41] S.-J. Park, H. Son, S. Cho, K.-S. Hong, and S. Lee, "Srfeat: Single image super-resolution with feature discrimination," in *Proceedings of the European conference on computer vision (ECCV)*, 2018, pp. 439–455.
- [42] X. Wang, K. Yu, S. Wu, J. Gu, Y. Liu, C. Dong, Y. Qiao, and C. Change Loy, "Esrgan: Enhanced super-resolution generative adversarial networks," in *Proceedings of the European conference on computer vision (ECCV) workshops*, 2018, pp. 0–0.
- [43] J.-Y. Zhu, T. Park, P. Isola, and A. A. Efros, "Unpaired image-to-image translation using cycle-consistent adversarial networks," in *Proceedings of the IEEE international conference on computer vision*, 2017, pp. 2223–2232.
- [44] M. Mirza and S. Osindero, "Conditional generative adversarial nets," *arXiv preprint arXiv:1411.1784*, 2014.
- [45] S. Reed, Z. Akata, X. Yan, L. Logeswaran, B. Schiele, and H. Lee, "Generative adversarial text to image synthesis," in *International conference on machine learning*. PMLR, 2016, pp. 1060–1069.
- [46] H. Zhang, T. Xu, H. Li, S. Zhang, X. Wang, X. Huang, and D. N. Metaxas, "Stackgan: Text to photo-realistic image synthesis with stacked generative adversarial networks," in *Proceedings of the IEEE international conference on computer vision*, 2017, pp. 5907–5915.
- [47] N. Bodla, G. Hua, and R. Chellappa, "Semi-supervised fusedgan for conditional image generation," in *Proceedings of the European conference on computer vision (ECCV)*, 2018, pp. 669–683.
- [48] Q. Lao, M. Havaei, A. Pesaranhader, F. Dutil, L. D. Jorio, and T. Fevens, "Dual adversarial inference for text-to-image synthesis," in *Proceedings of the IEEE/CVF International Conference on Computer Vision*, 2019, pp. 7567–7576.
- [49] W. Li, P. Zhang, L. Zhang, Q. Huang, X. He, S. Lyu, and J. Gao, "Object-driven text-to-image synthesis via adversarial training," in *Proceedings of the IEEE/CVF Conference on Computer Vision and Pattern Recognition*, 2019, pp. 12 174–12 182.
- [50] D. M. Souza, J. Wehrmann, and D. D. Ruiz, "Efficient neural architecture for text-to-image synthesis," in *2020 International Joint Conference on Neural Networks (IJCNN)*. IEEE, 2020, pp. 1–8.
- [51] Z. Wang, Z. Quan, Z.-J. Wang, X. Hu, and Y. Chen, "Text to image synthesis with bidirectional generative adversarial network," in *2020 IEEE International Conference on Multimedia and Expo (ICME)*. IEEE, 2020, pp. 1–6.
- [52] H. Zhang, J. Y. Koh, J. Baldridge, H. Lee, and Y. Yang, "Cross-modal contrastive learning for text-to-image generation," in *Proceedings of the IEEE/CVF conference on computer vision and pattern recognition*, 2021, pp. 833–842.
- [53] A. Ramesh, M. Pavlov, G. Goh, S. Gray, C. Voss, A. Radford, M. Chen, and I. Sutskever, "Zero-shot text-to-image generation," in *International Conference on Machine Learning*. PMLR, 2021, pp. 8821–8831.
- [54] J. Atwood and D. Towsley, "Diffusion-convolutional neural networks," *Advances in neural information processing systems*, vol. 29, 2016.
- [55] C. Saharia, W. Chan, S. Saxena, L. Li, J. Whang, E. L. Denton, K. Ghasemipour, R. Gontijo Lopes, B. Karagol Ayan, T. Salimans *et al.*, "Photorealistic text-to-image diffusion models with deep language understanding," *Advances in Neural Information Processing Systems*, vol. 35, pp. 36 479–36 494, 2022.
- [56] D. M. J. T. R. S. N. Sebastian, "Midjourney," 2023. [Online]. Available: <https://www.midjourney.com/home/?callbackUrl=%2Fapp%2F>
- [57] R. Corvi, D. Cozzolino, G. Zingarini, G. Poggi, K. Nagano, and L. Verdoliva, "On the detection of synthetic images generated by diffusion models," in *ICASSP 2023-2023 IEEE International Conference on Acoustics, Speech and Signal Processing (ICASSP)*. IEEE, 2023, pp. 1–5.
- [58] Z. Sha, Z. Li, N. Yu, and Y. Zhang, "De-fake: Detection and attribution of fake images generated by text-to-image diffusion models," *arXiv preprint arXiv:2210.06998*, 2022.
- [59] K. He, X. Zhang, S. Ren, and J. Sun, "Deep residual learning for image recognition," in *Proceedings of the IEEE conference on computer vision and pattern recognition*, 2016, pp. 770–778.
- [60] D. A. Coccomini, A. Esuli, F. Falchi, C. Gennaro, and G. Amato, "Detecting images generated by diffusers," *arXiv preprint arXiv:2303.05275*, 2023.
- [61] L. Guarnera, O. Giudice, and S. Battiato, "Level up the deepfake detection: a method to effectively discriminate images generated by gan architectures and diffusion models," *arXiv preprint arXiv:2303.00608*, 2023.
- [62] R. Amoroso, D. Morelli, M. Cornia, L. Baraldi, A. Del Bimbo, and R. Cucchiara, "Parents and children: Distinguishing multimodal deepfakes from natural images," *arXiv preprint arXiv:2304.00500*, 2023.
- [63] H. Wu, J. Zhou, and S. Zhang, "Generalizable synthetic image detection via language-guided contrastive learning," *arXiv preprint arXiv:2305.13800*, 2023.
- [64] Z. Xi, W. Huang, K. Wei, W. Luo, and P. Zheng, "Ai-

- generated image detection using a cross-attention enhanced dual-stream network,” *arXiv preprint arXiv:2306.07005*, 2023.
- [65] P. Lorenz, R. Durall, and J. Keuper, “Detecting images generated by deep diffusion models using their local intrinsic dimensionality,” *arXiv preprint arXiv:2307.02347*, 2023.
- [66] Y. Ju, S. Jia, J. Cai, H. Guan, and S. Lyu, “Glff: Global and local feature fusion for ai-synthesized image detection,” *IEEE Transactions on Multimedia*, 2023.
- [67] S. Sinitisa and O. Fried, “Deep image fingerprint: Accurate and low budget synthetic image detector,” *arXiv preprint arXiv:2303.10762*, 2023.
- [68] X. Guo, X. Liu, Z. Ren, S. Grosz, I. Masi, and X. Liu, “Hierarchical fine-grained image forgery detection and localization,” in *Proceedings of the IEEE/CVF Conference on Computer Vision and Pattern Recognition (CVPR)*, June 2023, pp. 3155–3165.
- [69] D. Cozzolino, G. Poggi, R. Corvi, M. Nießner, and L. Verdoliva, “Raising the bar of ai-generated image detection with clip,” *arXiv preprint arXiv:2312.00195*, 2023.
- [70] Z. Wang, J. Bao, W. Zhou, W. Wang, H. Hu, H. Chen, and H. Li, “Dire for diffusion-generated image detection,” *arXiv preprint arXiv:2303.09295*, 2023.
- [71] R. Ma, J. Duan, F. Kong, X. Shi, and K. Xu, “Exposing the fake: Effective diffusion-generated images detection,” *arXiv preprint arXiv:2307.06272*, 2023.
- [72] M. Goljan, J. Fridrich, and R. Cogranne, “Rich model for steganalysis of color images,” in *2014 IEEE International workshop on information forensics and security (WIFS)*. IEEE, 2014, pp. 185–190.
- [73] A. Odena, V. Dumoulin, and C. Olah, “Deconvolution and checkerboard artifacts,” *Distill*, vol. 1, no. 10, p. e3, 2016.
- [74] H. Li, B. Li, S. Tan, and J. Huang, “Identification of deep network generated images using disparities in color components,” *Signal Processing*, vol. 174, p. 107616, 2020.
- [75] K. Chandrasegaran, N.-T. Tran, A. Binder, and N.-M. Cheung, “Discovering transferable forensic features for cnn-generated images detection,” in *European Conference on Computer Vision*. Springer, 2022, pp. 671–689.
- [76] E. J. Hu, Y. Shen, P. Wallis, Z. Allen-Zhu, Y. Li, S. Wang, L. Wang, and W. Chen, “Lora: Low-rank adaptation of large language models,” *arXiv preprint arXiv:2106.09685*, 2021.
- [77] J. Deng, W. Dong, R. Socher, L.-J. Li, K. Li, and L. Fei-Fei, “Imagenet: A large-scale hierarchical image database,” in *2009 IEEE conference on computer vision and pattern recognition*. Ieee, 2009, pp. 248–255.
- [78] D. P. Kingma and J. Ba, “Adam: A method for stochastic optimization,” *arXiv preprint arXiv:1412.6980*, 2014.
- [79] Z. Wang, H. Zheng, P. He, W. Chen, and M. Zhou, “Diffusion-gan: Training gans with diffusion,” *arXiv preprint arXiv:2206.02262*, 2022.
- [80] A. Sauer, K. Chitta, J. Müller, and A. Geiger, “Projected gans converge faster,” *Advances in Neural Information Processing Systems*, vol. 34, pp. 17 480–17 492, 2021.
- [81] U. Ojha, Y. Li, and Y. J. Lee, “Towards universal fake image detectors that generalize across generative models,” 2023.
- [82] S.-Y. Wang, O. Wang, R. Zhang, A. Owens, and A. A. Efros, “Cnn-generated images are surprisingly easy to spot... for now,” in *Proceedings of the IEEE/CVF conference on computer vision and pattern recognition*, 2020, pp. 8695–8704.